Hindawi
Shock and Vibration
Volume 2021, Article ID 5574325, 9 pages
https://doi.org/10.1155/2021/5574325

Research Article

Effect of Joint Density on Rockburst Proneness of the Elastic-Brittle-Plastic Rock Mass

Jiliang Pan,[1,2,3] **Fenhua Ren**,[1,2,3] **and Meifeng Cai**[1,2,3]

[1]*School of Civil and Resource Engineering, University of Science and Technology Beijing, Beijing 100083, China*
[2]*Key Laboratory of High-Efficient Mining and Safety of Metal Mines (Ministry of Education of China), University of Science and Technology Beijing, Beijing 100083, China*
[3]*Beijing Key Laboratory of Urban Underground Space Engineering, University of Science and Technology Beijing, Beijing 100083, China*

Correspondence should be addressed to Fenhua Ren; renfh_2001@163.com

Received 1 February 2021; Revised 27 February 2021; Accepted 10 March 2021; Published 17 March 2021

Academic Editor: chao xu

The prediction of rockburst proneness is the basis of preventing and controlling rockburst disasters in rock engineering. Based on energy theory and damage mechanics, the quantitative functional relationship between joint density and energy density was derived. Then, the theoretical results were verified by numerical simulation and uniaxial compression test, and the effect of joint density on rockburst proneness of the elastic-brittle-plastic rock mass was discussed. The results show that the relationship between the joint density and the dissipated energy index of the jointed rock mass is a logarithmic function. With the same total input energy, the higher the joint density, the more the damage dissipation energy. Even in the case of high joint density, the rock mass still has limited resistance to external failure. Under the same joint density, the strength of parallel jointed rock mass is better than that of the cross-jointed rock mass, and the parallel jointed rock mass can accumulate more elastic strain energy and has higher rockburst proneness. The joint density is closely related to the ability of the rock mass to store high strain energy. The higher the joint density is, the weaker the ability to accumulate the elastic strain energy of rock mass is and the lower the rockburst proneness is. It is helpful to predict rockburst proneness by investigating and studying the properties of geological discontinuities. The research results have some theoretical and engineering guiding significance for the prediction of rockburst proneness of the jointed rock mass.

1. Introduction

As in situ stresses increase with depth, stress-induced rock fracturing, especially the sudden and violent failure of rock, will be a great threat to the safety of underground construction, which has attracted the widespread attention of researchers [1–6]. Spalling and rockburst are two common failure modes in deep hard-rock tunnels [7, 8]. Rock spalling, embodied as parallel fractures close to the free surface, is a tensional and brittle splitting failure process with no obvious ejection performance [2, 9, 10]. Different from the static failure mode of spalling, rockburst is a kind of artificial earthquake induced by human activities, such as mining excavations [4–6, 11, 12]. After the excavation of the roadway or stope, the stress of the surrounding rock will be redistributed, resulting in stress concentration. Before the failure of the rock mass, a large amount of elastic strain energy will accumulate in the stress concentration area. When the elastic strain energy is released suddenly in the free face, the rock will produce violent brittle failure in a short time, causing serious dynamic disasters [13–15]. Rock mass with rockburst proneness is usually elastic-perfectly brittle rock mass with few cracks or only hidden cracks [4, 16, 17]. In practice, most underground projects are built in a rock mass with structural planes. Numerous studies and production practices have shown that joints, faults, folds, and other geological structures are some of the important factors causing rockburst [18–20]. At the same time, rockburst prediction has been one of the biggest challenges in the field of rock mechanics for its nature of

unpredictability [21, 22]. Gong et al. [23] proposed that the mechanism of spalling damage on inducing rockburst is mainly embodied in two aspects: promoting large buckling deformations (providing energy for rockburst) and weakening the strength of the rock mass (creating conditions for the sudden release of energy).

The failure behavior of jointed rock mass under different stress environments is highly complex [24–26]. The initial crack or local high stress will damage the rock mass and reduce its strength. However, there are still undamaged areas in the rock mass, which make the rock mass have a certain bearing capacity. It is difficult for general strength theory and failure criterion to effectively reflect the strength characteristics and failure mechanism [27, 28]. The failure of the engineering rock mass is actually a process of energy accumulation, transfer, and dissipation, and the transformation of energy is an essential feature of the material physical process [11, 24, 29–31]. It has become a hot topic to study the instability and failure behavior of rock mass based on the energy theory. For understanding the rockburst mechanism, Cai [11] proposed two necessary conditions for the occurrence of rockburst: (1) the rock mass has the capability to store a great amount of energy and possesses a strong bumping-prone characteristic when damaged; and (2) the geological conditions in the mining area have favorable geostress environments that can form high-stress concentration area and accumulate great energy.

In recent years, it has been widely accepted that strain energy stored in rock masses plays an important role in inducing rockburst. Jiang et al. [32] summarized some typical characteristics of rockburst and found that the internal cause of rockburst was energy release. Then, they proposed a new energy index, the local energy release rate, to simulate the conditions causing rockburst and simulated the brittle breakage of Mine-by tunnel rock in Canada and two rockbursts in the Jinping pilot tunnels. Based on energy theory, Gong et al. [33, 34] proposed a peak-strength strain energy storage index for estimating and classifying the rockburst proneness of rock materials. Based on in situ investigations of the tunnels at Jinping II hydropower station, Hou et al. [35] qualitatively analyzed the mechanism of tensile spalling rockburst in deep-buried intact marble. On the other hand, numerical simulation has become one of the main research methods in the study of rock mass deformation and rockburst hazard [36–39]. For example, Gao et al. [36] introduced a novel distinct element bonded block method using the commercial code UDEC to simulate rockbursts. Using the RFPA software, Zhu et al. [37] proposed a numerical model capable of studying the dynamic failure process of rock under coupled static geostress and dynamic disturbance.

Compared with intact rock mass, the study on rockburst proneness of jointed rock mass is less. However, joints or fissures exist widely in engineering rock mass, and the effect of joints on rockburst should be considered. At present, the research on the joint density of rock mass is mostly focused on the intermittent joints with a small number (several or dozens of joints) [40–42]. Limited by the size effect and test conditions, the research results of jointed rock samples cannot well reflect the relationship between joint density and rock strength, nor the effect of joint density on rockburst. Based on energy theory and damage mechanics, this paper analytically assesses the effect of joint density on predicting the energy released and dissipated in a rock mass and derives the quantitative functional relationship between joint density and energy density. Then, the numerical models of parallel jointed rock mass and cross-jointed rock mass are established by the three-dimensional distinct element code (3DEC). The theoretical results are verified by numerical simulation and uniaxial compression test. Finally, the relationship between joint density and elastic strain energy is discussed, and the effect of joint density on the rockburst proneness of the elastic-brittle-plastic rock mass is revealed.

2. Calculation Method of Energy

2.1. Simplified Model. As the rockburst is a typical brittle failure, an elastic-brittle-plastic mode is needed to describe the outburst activity of the surrounding rock. The main characteristics of the stress-strain curve of elastic-brittle-plastic materials are as follows [43, 44]:

(1) The curve before the peak is approximately linear.

(2) There is almost no yield plateau at the peak.

(3) The curve drops sharply to the residual value at the peak.

(4) There is no stress fluctuation in the postpeak stage.

Based on the above characteristics, we simplified the yield plateau as a point at the peak, linearized the elastic stage and brittle drop stage, and ignored the slope of the brittle decline stage and the strengthening or attenuation of the residual stress. Therefore, the rock can be regarded as an ideal elastic-brittle material, and its constitutive model can be divided into three stages [45]: linear elasticity, brittle stress drop, and plastic flow. The material behavior of the simplified elastic-brittle-plastic model used in this study is shown in Figure 1. In linear elastic deformation stage (OA), the deformation obeys Hooke's law of elasticity. In the brittle failure stage (AB), it is assumed that the failure of rock materials obeys the Mohr-Coulomb criterion. In plastic flow stage (BC), the strength of rock decreases to the residual strength and remains unchanged, while the plastic deformation increases continuously.

2.2. Energy Principle. The ideal elastic-brittle rock mass with joints can be regarded as composed of joints and intact rock mass. According to the second law of thermodynamics, the damage dissipation energy is irreversible, and the input energy will be completely dissipated in the damage region. Because the rock element in the joint damage region is unable to store elastic strain energy, the total strain energy produced by the external force can only be stored in the undamaged rock mass. The initial damage of rock materials caused by joints is closely related to the joint density. Different from jointed rock mass, there is no initial damage caused by joints in the intact elastic-brittle rock material, and the work done by the external force is completely transformed into elastic strain energy stored in the rock mass [28–30].

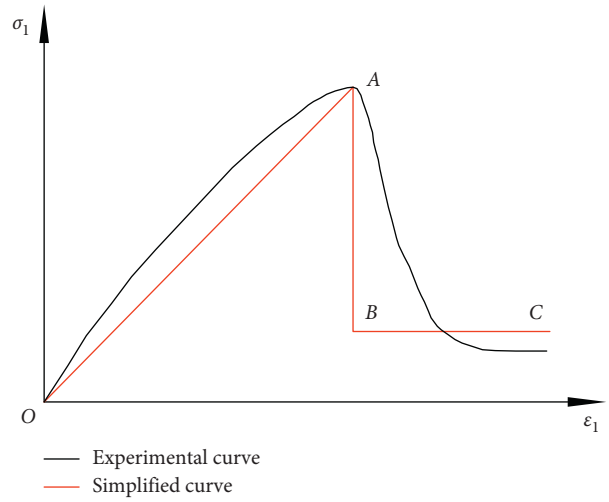

Figure 1: Stress-strain relationship of the simplified elastic-brittle-plastic model.

Based on the energy theory, the failure of rock material is the result of energy conversion. Assuming that a unit volume of material deforms by outer forces and this physical process occurs in a closed system, the energy conversion can be defined according to the first law of thermodynamics as

$$U^{\text{tot}} = U^e + U^d, \tag{1}$$

where U^e and U^d are the elastic strain energy density and dissipation energy density, respectively. U^{tot} is the energy density done by the outer force, which can be calculated by

$$U^{\text{tot}} = \int_0^{\varepsilon_1} \sigma_1 \mathrm{d}\varepsilon_1 + \int_0^{\varepsilon_2} \sigma_2 \mathrm{d}\varepsilon_2 + \int_0^{\varepsilon_3} \sigma_3 \mathrm{d}\varepsilon_3, \tag{2}$$

where σ_i and ε_i $(i = 1, 2, 3)$ are the total stress and strain in the three principal stress directions, respectively. Under uniaxial compression conditions, equation (2) can be written as

$$U^{\text{tot}} = \int_0^{\varepsilon_1} \sigma_1 \mathrm{d}\varepsilon_1, \tag{3}$$

where σ_1 and ε_1 are the axial stress and axial strain of the rock element, respectively.

It can be seen from equation (3) that the elastic strain energy can be calculated by integrating the stress-strain curve. The existence of joints will reduce the ability of the rock mass to bear the compression load, which is reflected in two aspects: one is that, under the same load, the deformation of the jointed rock mass is greater than that of the intact rock mass; the other is that the peak strength of the jointed rock mass is less than that of the intact rock mass.

The relationship between the elastic strain energy and the dissipation energy in the rock mass element is shown in Figure 2. In the figure, $\mathrm{d}\varepsilon$ is the unit strain increment; σ^c is the peak stress in the calculation area; the footnotes t and j represent the intact and jointed rock mass, respectively; and ΔU_j^e and ΔU_j^d are the unit elastic energy increment and unit dissipative energy increment of jointed rock mass, respectively.

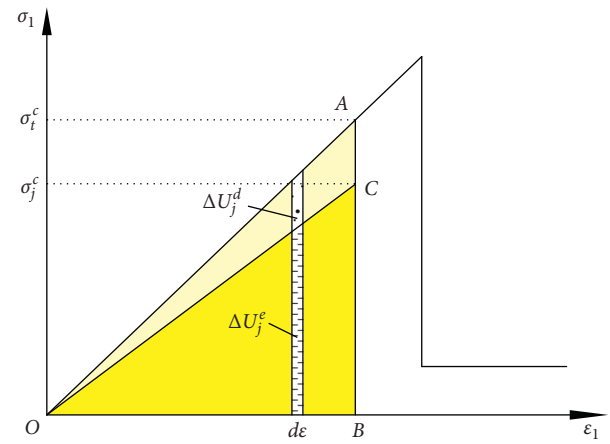

Figure 2: The relationship between elastic strain energy and dissipation energy.

For the intact rock mass, the yellow area in Figure 2 is the total input energy accumulated in the calculation area. The total input energy is equal to the elastic strain energy because it is not affected by joint damage. For the jointed rock mass, a part of the total input energy is stored in the rock mass in the form of elastic strain energy, and a part is lost in the form of dissipated energy due to the damage caused by joints. The dark yellow area in Figure 2 is the elastic strain energy accumulated in the undamaged region of the jointed rock mass, and the light yellow area is the energy dissipated in the joint damaged region.

The stress-strain curve before the peak strain is divided into n equal parts. According to the principle of definite integral, the total energy density of the rock element under uniaxial compression can be expressed as

$$U^{\text{tot}} = \lim_{n \longrightarrow \infty} \sum_{i=1}^{n} \frac{1}{2} \left(\sigma_t^i + \sigma_t^{i+1} \right) \mathrm{d}\varepsilon. \tag{4}$$

Furthermore, the elastic strain energy of the jointed rock element under uniaxial compression can be expressed as

$$U_j^e = \lim_{n \longrightarrow \infty} \sum_{i=1}^{n} \frac{1}{2} \left(\sigma_j^i + \sigma_j^{i+1} \right) \mathrm{d}\varepsilon, \tag{5}$$

where U^{tot} is the total energy increment of the intact and jointed sample, U_j^e is the elastic strain energy increment of the jointed sample, σ^i and σ^{i+1} are the corresponding stresses of the ith and the $(i+1)$th interval in equal parts, and the footnotes t and j represent the intact and jointed samples respectively.

3. Joint Density-Energy Density Relation Equation

The mechanical properties of the jointed rock mass are closely related to the joint density, which is defined as the number of joints contained in the unit volume of the jointed rock mass. The macrophenomenological method can be used to establish damage variables, which indirectly reflect the damage extent of rock mass caused by joints.

Considering that the change of elastic modulus of the rock mass is easy to obtain, based on the macrophenomenal damage mechanics, the damage variable of the jointed rock mass can be defined as

$$D = 1 - \frac{E_j}{E_t} = 1 - \lambda, \tag{6}$$

where E_j and E_t are the elastic moduli of jointed and intact rock mass, respectively, and the ratio of E_j to E_t is a dimensionless constant expressed by λ, which is defined as the equivalent modulus.

Because we assume that the rock mass is an elastic-brittle-plastic material, E_j and E_t can be calculated by the following equation:

$$E_t = \frac{\partial \sigma_t}{\partial \varepsilon}. \tag{7}$$

According to the energy principle, there is the following equation between the energy increments of jointed rock mass:

$$\Delta U_j^e = \Delta U^{\text{tot}} - \Delta U_j^d. \tag{8}$$

For intact and jointed rock samples with the same energy input, the expressions of elastic strain energy increment and total energy increment can be obtained from equations (4) and (5) as follows:

$$\begin{aligned} \Delta U^{\text{tot}} &= \frac{1}{2}\left(\sigma_t^i + \sigma_t^{i+1}\right)\mathrm{d}\varepsilon, \\ \Delta U_j^e &= \frac{1}{2}\left(\sigma_j^i + \sigma_j^{i+1}\right)\mathrm{d}\varepsilon. \end{aligned} \tag{9}$$

If $\mathrm{d}\varepsilon \longrightarrow 0$, there are

$$\begin{aligned} \sigma_t^i \approx \sigma_t^{i+1} &= \frac{\Delta U^{\text{tot}}}{\mathrm{d}\varepsilon}, \\ \sigma_j^i \approx \sigma_j^{i+1} &= \frac{\Delta U_j^e}{\mathrm{d}\varepsilon} = \frac{\Delta U^{\text{tot}} - \Delta U_j^d}{\mathrm{d}\varepsilon}. \end{aligned} \tag{10}$$

Because of $\lim_{\mathrm{d}\varepsilon \longrightarrow 0} \Delta\sigma_j = 0$ and $\lim_{\mathrm{d}\varepsilon \longrightarrow 0} \Delta\sigma_t = 0$, we can get the following equations:

$$\begin{aligned} E_t &= \frac{\partial \sigma_t}{\partial \varepsilon} = \frac{\partial\left(\Delta U^{\text{tot}}\right)/\mathrm{d}\varepsilon}{\partial \varepsilon}, \\ E_j &= \frac{\partial \sigma_j}{\partial \varepsilon} = \frac{\partial\left(\Delta U^{\text{tot}} - \Delta U_j^d\right)/\mathrm{d}\varepsilon}{\partial \varepsilon}. \end{aligned} \tag{11}$$

Furthermore, it is clear that

$$\begin{aligned} \frac{\Delta U^{\text{tot}}}{\mathrm{d}\varepsilon} &= \frac{\left(U^{\text{tot}}\right)^{i+1} - \left(U^{\text{tot}}\right)^i}{\mathrm{d}\varepsilon} = \frac{\partial U^{\text{tot}}}{\partial \varepsilon}, \\ \frac{\Delta U_j^d}{\mathrm{d}\varepsilon} &= \frac{\left(U_j^d\right)^{i+1} - \left(U_j^d\right)^i}{\mathrm{d}\varepsilon} = \frac{\partial U_j^d}{\partial \varepsilon}. \end{aligned} \tag{12}$$

Therefore, the expression of the equivalent modulus can be calculated by

$$\lambda = \frac{E_j}{E_t} = 1 - \frac{\partial^2 U_j^d / \partial \varepsilon^2}{\partial^2 U^{\text{tot}} / \partial \varepsilon^2}. \tag{13}$$

Furthermore, it is assumed that there is an exponential function relationship between the joint density and the damage variable [46]:

$$\rho = e^{(1/\psi)D}, \tag{14}$$

where ρ is the joint density per unit volume of rock and ψ is the damping factor.

Considering that the joint density of the rock elements is always greater than 0, equation (14) can be written as follows:

$$D = \psi \ln \rho. \tag{15}$$

Thus, we can get

$$\psi \ln \rho \frac{\partial^2 U^{\text{tot}}}{\partial \varepsilon^2} = \frac{\partial^2 U_j^d}{\partial \varepsilon^2}. \tag{16}$$

By integrating with both parts of the equation:

$$\psi \ln(\rho) U^{\text{tot}} = U_j^d + C_1 \mathrm{d}\varepsilon + C_2, \tag{17}$$

where C_1 and C_2 are the constants obtained by integral.

Since $\mathrm{d}\varepsilon$ is an infinitesimal quantity, $C_1\mathrm{d}\varepsilon$ can be ignored. Equation (17) can be represented by

$$\frac{U_j^d}{U^{\text{tot}}} = \psi \ln \rho - \frac{1}{U^{\text{tot}}} C_2. \tag{18}$$

Due to the fact that input total energy U^{tot} is a given, C_2/U^{tot} can be regarded as a constant C. The quantitative relationship between strain energy, dissipation energy, and joint density is obtained as follows:

$$\frac{U_j^d}{U^{\text{tot}}} = \psi \ln \rho - C. \tag{19}$$

It can be seen from equation (19) that when the total energy input from the outside is the same, the greater the joint density is, the more the damage dissipation energy is and the weaker the ability of rock mass to store elastic strain energy is.

4. Numerical Analysis and Validation

4.1. Numerical Calculation Model. To obtain the basic mechanical parameters of the numerical model, some intact cylindrical monzonitic granite was selected for the uniaxial compression test and shear test. The samples used in the experiments are collected from Sanshandao Gold Mine, which is an underground gold mine located in Laizhou city, Shandong province, China. According to the average value of the test results, the mechanical parameters of rock samples are obtained, as shown in Table 1. Moreover, it is very difficult to choose reasonable stiffness parameters of the structural plane in numerical analysis of rock mass using numerical simulation software [47, 48]. Considering that the purpose of this paper is to obtain the relationship between joint density and energy index, it is necessary to ensure that

Table 1: Mechanical properties of rock samples.

Elastic modulus E (GPa)	Poisson's ratio υ	Cohesion c (MPa)	Internal friction angle φ (°)	Compressive strength σ_t (MPa)
21.16	0.226	26.54	33.21	60.62

jointed samples have a strong ability to resist failure. Therefore, on the premise of not affecting the calculation results of energy index, the compressive capacity of jointed rock mass model can be effectively guaranteed by selecting larger structural plane stiffness parameters. The selected mechanical parameters of structural plane are shown in Table 2.

To validate the proposed analytical method, the 3DEC software is used to carry out uniaxial compression tests on jointed rock samples. Several numerical studies have been carried out on 1 m × 1 m × 1 m cubic rock samples with different joint densities. The joints included in the samples are transfixion joints, which are divided into parallel joints and cross joints for analysis. The number of joints in each group is 10, 20, 30, 40, 50, 60, 70, 80, 90, 100, 120, 140, 160, 180, 200, 300, and 400, respectively. The Mohr-Coulomb strain-softening model is selected as the block constitutive model to reflect the strength reduction characteristics of rock after reaching the peak strength, and the Coulomb Slip model is selected as the joint constitutive model to reflect the compressive and shear action between the contact surfaces of blocks. The numerical calculation models are established as shown in Figure 3.

The top of the model is the loading boundary and the bottom is the fixed boundary. To ensure that the total energy input of each sample is consistent, a displacement of 0.1 cm/s is applied downward from the loading boundary through the displacement control. Record the force and displacement at the top of the model in each time step, and the product of the two is the work done by the external force. According to the law of energy conservation, the work done by the external force is equal to the energy input into the rock mass. The total energy input can be obtained by the superposition of the work done by the external force in each time step. The purpose of this paper is to investigate the effect of joint density on energy dissipation, so it is necessary to ensure that the simulated jointed rock mass does not produce macroscopic brittle failure. Combined with the stress-strain curve of the intact rock mass, 10 kJ is selected as the threshold of total energy input. When the threshold value is reached, the calculation is terminated to ensure that each jointed sample is in the stage of elastic strain energy accumulation during uniaxial compression.

4.2. Simulation Results. By superposing the elastic strain energy of each monitoring unit, the elastic strain energy stored in the rock sample can be obtained. The ratio of dissipated energy to total input energy is defined as the dissipated energy index. The numerical calculation results of rock samples with different joint densities obtained by using the energy characteristic analysis method are shown in Table 3. The relation curve between dissipation energy index and joint density is shown in Figure 4. As illustrated, there is a good agreement between the numerical and analytical solutions. For parallel joints' and cross joints' samples, the relationship between the dissipated energy index and the joint density is the logarithmic function given in equation (18), and the specific fitting functions are as follows.

For parallel joints' samples,

$$y = 0.1818 \ln(x) - 0.3635, \quad R^2 = 0.9916. \tag{20}$$

For cross joints' samples,

$$y = 0.2122 \ln(x) - 0.4074, \quad R^2 = 0.9936. \tag{21}$$

It can also be seen from Figure 4 that, with the increase of joint density, the dissipation energy index becomes larger and larger but eventually tends to a constant value less than 1. This changing trend shows that, even in the case of high joint density, the rock mass still has limited resistance to external failure, and the ability of rock mass with parallel joints is stronger than that with cross joints.

5. Discussion

According to the principle of energy, when the strength of rock mass itself cannot resist the work of external force, the elastic strain energy gathered in the rock mass will be released in an instant, and the rock mass will show brittle failure in a short time, which is represented by rockburst macroscopically. Through the calculation and analysis of the local releasable elastic strain energy of rock mass, we can better understand the rockburst proneness of the jointed rock mass.

To deeply analyze the relationship between elastic strain energy and joint density, the logarithmic function is used to fit the experimental data. Through comparative analysis, the fitting curve of the logarithmic function is consistent with the experimental results (the coefficient of determination $R^2 > 0.99$). The relationship between joint density and elastic strain energy is shown in Figure 5. It can be seen that the larger the joint density, the weaker the ability of rock mass to accumulate elastic strain energy, which also means the lower the rockburst proneness. Under the same joint density, the rock mass is more broken due to the smaller volume of the rock blocks divided by the cross joints. Compared with parallel joints, rock mass with cross joints can accumulate less elastic strain energy and is less prone to rockburst. The fitting functions between the joint density and the elastic strain energy for parallel joints' and cross joints' samples are as follows.

For parallel joints' samples,

Table 2: Mechanical parameters of structural surfaces.

Normal stiffness (K_n/GPa·m^{-1})	Shear stiffness (K_s/GPa·m^{-1})	Cohesion c_i (MPa)	Internal friction angle φ_i (°)
90	70	13	36

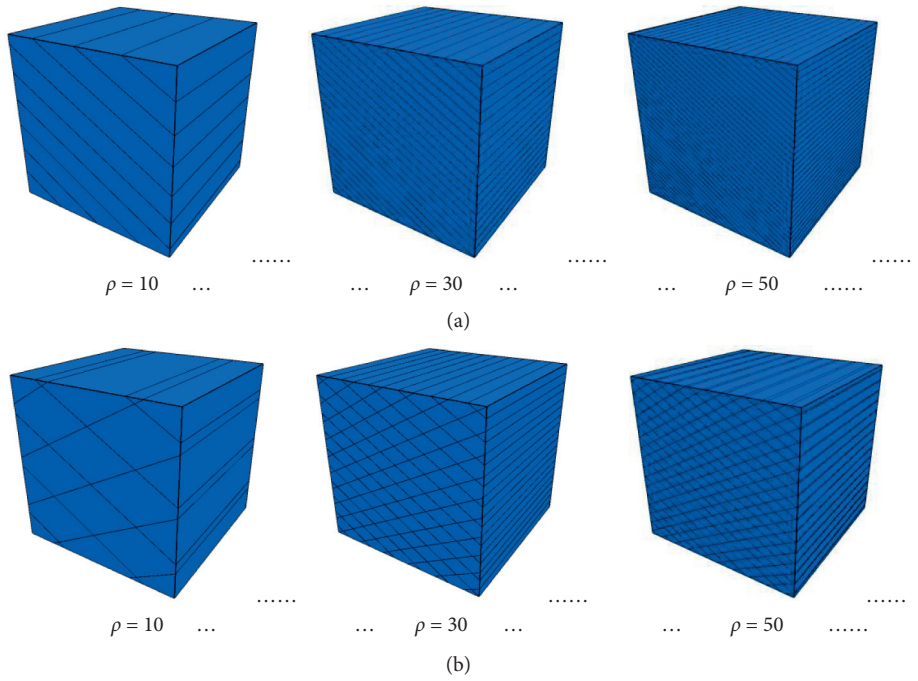

Figure 3: Numerical calculation model. (a) Parallel joints' samples and (b) cross joints' samples.

Table 3: Energy analysis of rock samples with different joint densities.

Joint density	Parallel joints			Cross joints		
	Elastic energy (J)	Dissipated energy (J)	Dissipated energy index	Elastic energy (J)	Dissipated energy (J)	Dissipated energy index
10	8988	1012	0.10	8772	1228	0.12
20	8269	1731	0.17	7856	2144	0.21
30	7687	2313	0.23	7085	2915	0.29
40	7095	2905	0.29	6479	3521	0.35
50	6688	3312	0.33	5963	4037	0.40
60	6336	3664	0.37	5530	4470	0.45
70	6003	3997	0.40	5078	4922	0.49
80	5720	4280	0.43	4768	5232	0.52
90	5523	4477	0.45	4481	5519	0.55
100	5236	4764	0.48	4173	5827	0.58
120	4891	5109	0.51	3812	6188	0.62
140	4568	5432	0.54	3473	6527	0.65
160	4301	5699	0.57	3194	6806	0.68
180	4099	5901	0.59	2978	7022	0.70
200	3881	6119	0.61	2756	7244	0.72
300	3212	6788	0.68	1992	8008	0.80
400	2763	7237	0.72	1464	8536	0.85

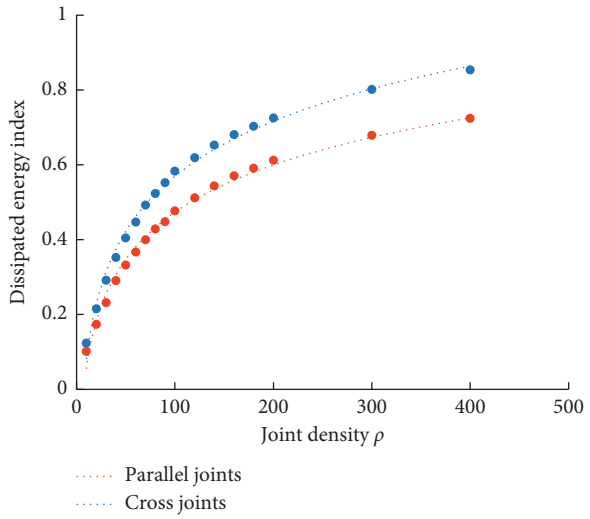

Figure 4: Relationship between dissipated energy ratio and joint density.

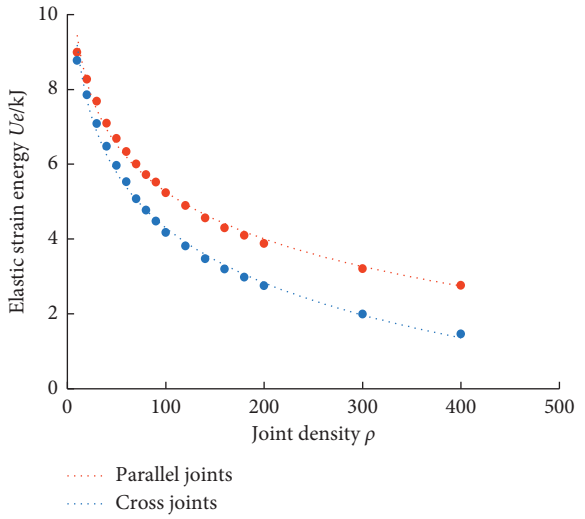

Figure 5: Relationship between elastic strain energy and joint density.

$$y = -1.818 \ln(x) + 13.635,$$
$$R^2 = 0.9916. \quad (22)$$

For cross joints' samples:

$$y = -2.122 \ln(x) + 14.074,$$
$$R^2 = 0.9936. \quad (23)$$

The ratio of elastic strain energy of cross-jointed rock to that of parallel jointed rock under different joint density is shown in Figure 6. It can be seen that the elastic strain energy ratio is approximately linear with the joint density, and the fitting function is as follows:

$$y = -0.1107x + 93.83,$$
$$R^2 = 0.957. \quad (24)$$

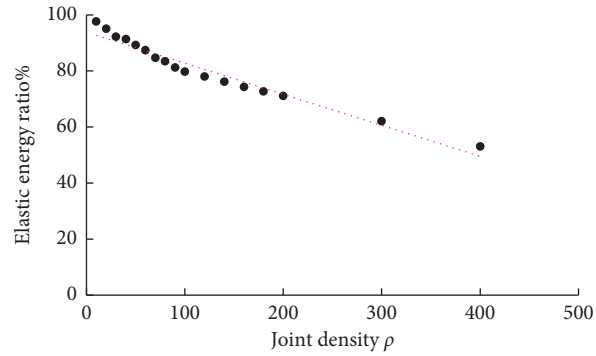

Figure 6: Relationship between elastic energy ratio and joint density.

When the joint density is small, the storage capacity of elastic strain energy is approximately the same, but with the increase of joint density, the relative energy storage capacity of cross-jointed rock will become weaker and weaker. For example, when the joint density is 100 per volume, the elastic strain energy stored in cross-jointed rock is about 80% of that in parallel jointed rock. When the joint density increases to 400 per volume, the energy storage capacity of cross-jointed rock mass is only about 50% of that of parallel joints. In other words, for well-developed joints, the rock mass with cross joints is less prone to rockburst than that with parallel joints of the same density. By studying the properties of discontinuities, the rockburst proneness can be better predicted.

It should be noted that there are still some weaknesses and limitations in this study. On the one hand, rockburst depends not only on the amount of elastic energy stored before the peak but also on the ability to release energy rapidly after the peak. The simplified elastic-brittle-plastic constitutive model is an idealized material behavior, which reduces the stress rapidly to the residual strength after the peak; that is, the rock mass has the ability to release energy quickly after the peak. Moreover, the weakening effect of joints on the strength parameters of rock mass is not considered in the model. On this basis, the relationship between the joint density and the elastic strain energy stored before the peak was discussed, which is considered to be the relationship between the joint density and rockburst proneness. On the other hand, this study is based on theoretical assumptions. The logarithmic function relationship between joint density and energy index is assumed in the theoretical analysis, and the purpose of numerical simulation is to verify this assumption. The preparation of jointed rock samples is difficult because of the high density of the transfixion joints. Therefore, in the research method, there is a lack of laboratory test verification and comparative analysis to prove that the logarithmic function fitting curve is more suitable for the test results.

6. Conclusion

Based on energy theory and damage mechanics, the quantitative functional relationship between joint density and energy density was derived. Then, the proposed analysis

method was verified by numerical simulation and uniaxial compression test, and the effect of joint density on rockburst proneness of the elastic-brittle-plastic rock mass was discussed. The main conclusions are as follows:

(1) The relationship between the joint density and the dissipated energy index of the elastic-brittle jointed rock mass is a logarithmic function. With the same total input energy, the higher the joint density, the more the damage dissipation energy. Even in the case of high joint density, the rock mass still has limited resistance to external failure.

(2) Under the same joint density, the strength of parallel jointed rock mass is better than that of cross-jointed rock mass, and the parallel jointed rock mass can accumulate more elastic strain energy and has higher rockburst proneness.

(3) The joint density is closely related to the ability of the rock to store high strain energy. The higher the joint density is, the weaker the ability to accumulate the elastic strain energy of rock mass is and the lower the rockburst proneness is. It is helpful to predict rockburst proneness by investigating and studying the properties of geological discontinuities.

Data Availability

The experimental data used to support the findings of this study are included within the article.

Conflicts of Interest

The authors declare that there are no conflicts of interest regarding the publication of this paper.

Acknowledgments

This research was funded by the Fundamental Research Funds of the Central Universities (no. FRF-TP-18-015A3) and the National Natural Science Foundation of China (nos. 51974014 and 52074020).

References

[1] W. D. Ortlepp and T. R. Stacey, "Rockburst mechanisms in tunnels and shafts," *Tunnelling and Underground Space Technology*, vol. 9, no. 1, pp. 59–65, 1994.

[2] Q. M. Gong, L. J. Yin, S. Y. Wu, J. Zhao, and Y. Ting, "Rock burst and slabbing failure and its influence on TBM excavation at headrace tunnels in Jinping II hydropower station," *Engineering Geology*, vol. 124, pp. 98–108, 2012.

[3] M. He, F. Ren, and D. Liu, "Rockburst mechanism research and its control," *International Journal of Mining Science and Technology*, vol. 28, no. 5, pp. 829–837, 2018.

[4] J. Deng and D. S. Gu, "Buckling mechanism of pillar rockbursts in underground hard rock mining," *Geomechanics and Geoengineering*, vol. 13, no. 3, pp. 168–183, 2018.

[5] F. Du, K. Wang, Y. Guo, G. Wang, L. Wang, and Y. Wang, "The mechanism of rockburst-outburst coupling disaster considering the coal-rock combination: an experiment study," *Geomechanics and Engineering*, vol. 22, no. 3, pp. 255–264, 2020.

[6] F. Du, K. Wang, X. Zhang, C. Xin, L. Shu, and G. Wang, "Experimental study of coal–gas outburst: insights from coal–rock structure, gas pressure and adsorptivity," *Natural Resources Research*, vol. 29, pp. 2481–2493, 2020.

[7] C. H. Dowding and C.-A. Andersson, "Potential for rock bursting and slabbing in deep caverns," *Engineering Geology*, vol. 22, no. 3, pp. 265–279, 1986.

[8] Y. Luo, F. Gong, D. Liu, S. Wang, and X. Si, "Experimental simulation analysis of the process and failure characteristics of spalling in D-shaped tunnels under true-triaxial loading conditions," *Tunnelling and Underground Space Technology*, vol. 90, pp. 42–61, 2019.

[9] Q. Jiang, X.-T. Feng, Y. Fan et al., "In situ experimental investigation of basalt spalling in a large underground powerhouse cavern," *Tunnelling and Underground Space Technology*, vol. 68, pp. 82–94, 2017.

[10] F. Gong, W. Wuxing, T. Li, and X. Si, "Experimental simulation and investigation of spalling failure of rectangular tunnel under different three-dimensional stress states," *International Journal of Rock Mechanics and Mining Sciences*, vol. 122, Article ID 104081, 2019.

[11] M. Cai, "Prediction and prevention of rockburst in metal mines - a case study of Sanshandao gold mine," *Journal of Rock Mechanics and Geotechnical Engineering*, vol. 8, no. 2, pp. 204–211, 2016.

[12] C. Xu, Q. Fu, X. Cui, K. Wang, Y. Zhao, and Y. Cai, "Apparent-depth effects of the dynamic failure of thick hard rock strata on the underlying coal mass during underground mining," *Rock Mechanics and Rock Engineering*, vol. 52, no. 5, pp. 1565–1576, 2019.

[13] J.-A. Wang and H. D. Park, "Comprehensive prediction of rockburst based on analysis of strain energy in rocks," *Tunnelling and Underground Space Technology*, vol. 16, no. 1, pp. 49–57, 2001.

[14] M. M. He, Z. Q. Zhang, J. W. Zhu, and N. Li, "Investigation of nonlinear energy dissipation and storage characteristics for evaluating rockburst proneness of granite and sandstone," *AIP Advances*, vol. 10, no. 9, p. 095316, 2020.

[15] L. Li and F. Gong, "Experimental investigation on the energy storage characteristics of red sandstone in triaxial compression tests with constant confining pressure," *Shock and Vibration*, vol. 2020, Article ID 8839761, 11 pages, 2020.

[16] E. B. Eberhardt, "Brittle rock fracture and progressive damage in uniaxial compression," Doctoral dissertation, University of Saskatchewan, Saskatoon, Canada, 1998.

[17] D. S. Cheon, S. Keon, C. Park, and C. Ryu, "An experimental study on the brittle failure under true triaxial conditions," *Tunnelling and Underground Space Technology*, vol. 21, no. 3, pp. 448-449, 2006.

[18] H. Zhou, F. Meng, C. Zhang, D. Hu, F. Yang, and J. Lu, "Analysis of rockburst mechanisms induced by structural planes in deep tunnels," *Bulletin of Engineering Geology and the Environment*, vol. 74, no. 4, pp. 1435–1451, 2015.

[19] X. G. Zhao, J. Wang, M. Cai et al., "Influence of unloading rate on the strainburst characteristics of Beishan granite under true-triaxial unloading conditions," *Rock Mechanics and Rock Engineering*, vol. 47, no. 2, pp. 467–483, 2014.

[20] C. Miao, X. Sun, Y. Zhang et al., "Experimental study on the strain rockburst of calcareous sandstone containing joint surface," *Arabian Journal of Geosciences*, vol. 13, no. 19, pp. 1–10, 2020.

[21] J. Zhou, X. Li, and X. Shi, "Long-term prediction model of rockburst in underground openings using heuristic algorithms and support vector machines," *Safety Science*, vol. 50, no. 4, pp. 629–644, 2012.

[22] J. Zhou, X. Li, and H. S. Mitri, "Evaluation method of rockburst: state-of-the-art literature review," *Tunnelling and Underground Space Technology*, vol. 81, pp. 632–659, 2018.

[23] F.-Q. Gong, Y. Luo, X.-B. Li, X.-F. Si, and M. Tao, "Experimental simulation investigation on rockburst induced by spalling failure in deep circular tunnels," *Tunnelling and Underground Space Technology*, vol. 81, pp. 413–427, 2018.

[24] J. Pan, X. Wu, Q. Guo, X. Xi, and M. Cai, "Uniaxial experimental study of the deformation behavior and energy evolution of conjugate jointed rock based on AE and DIC methods," *Advances in Civil Engineering*, vol. 2020, Article ID 8850250, 16 pages, 2020.

[25] Q. Guo, J. Pan, M. Cai, and Y. Zhang, "Investigating the effect of rock bridge on the stability of locked section slopes by the direct shear test and acoustic emission technique," *Sensors*, vol. 20, no. 3, p. 638, 2020.

[26] X. Xi, X. Wu, Q. Guo, and M. Cai, "Experimental investigation and numerical simulation on the crack initiation and propagation of rock with pre-existing cracks," *IEEE Access*, vol. 8, pp. 129636–129644, 2020.

[27] J. Pan, Z. Gao, and F. Ren, "Effect of strength criteria on surrounding rock of circular roadway considering strain softening and dilatancy," *Journal of the China Coal Society*, vol. 43, no. 12, pp. 3293–3301, 2018.

[28] H. P. Xie, Y. Ju, and L. Y. Li, "Criteria for strength and structural failure of rocks based on energy dissipation and energy release principles," *Chinese Journal of Rock Mechanics and Engineering*, vol. 24, no. 17, pp. 3003–3010, 2005.

[29] H. P. Xie, Y. Ju, L. Y. Li, and R. D. Peng, "Energy mechanism of deformation and failure of rock masses," *Chinese Journal of Rock Mechanics and Engineering*, vol. 27, no. 9, pp. 1729–1740, 2008.

[30] H. Xie, L. Li, R. Peng, and Y. Ju, "Energy analysis and criteria for structural failure of rocks," *Journal of Rock Mechanics and Geotechnical Engineering*, vol. 1, no. 1, pp. 11–20, 2009.

[31] Q. Guo, J. Pan, M. Cai, and Y. Zhang, "Analysis of progressive failure mechanism of rock slope with locked section based on energy theory," *Energies*, vol. 13, no. 5, p. 1128, 2020.

[32] Q. Jiang, X.-T. Feng, T.-B. Xiang, and G.-S. Su, "Rockburst characteristics and numerical simulation based on a new energy index: a case study of a tunnel at 2,500 m depth," *Bulletin of Engineering Geology and the Environment*, vol. 69, no. 3, pp. 381–388, 2010.

[33] F. Gong, J. Yan, X. Li, and S. Luo, "A peak-strength strain energy storage index for rock burst proneness of rock materials," *International Journal of Rock Mechanics and Mining Sciences*, vol. 117, pp. 76–89, 2019.

[34] F.-Q. Gong, Y.-L. Wang, and S. Luo, "Rockburst proneness criteria for rock materials: review and new insights," *Journal of Central South University*, vol. 27, no. 10, pp. 2793–2821, 2020.

[35] Z. S. Hou, Q. M. Gong, and Z. H. Sun, "Primary failure types and their failure mechanisms of deep buried and intact marble at Jinping II hydropower station," *Chinese Journal of Rock Mechanics and Engineering*, vol. 30, no. 4, pp. 727–732, 2011.

[36] F. Gao, P. K. Kaiser, D. Stead, E. Eberhardt, and D. Elmo, "Strainburst phenomena and numerical simulation of self-initiated brittle rock failure," *International Journal of Rock Mechanics and Mining Sciences*, vol. 116, pp. 52–63, 2019.

[37] W. C. Zhu, Z. H. Li, L. Zhu, and C. A. Tang, "Numerical simulation on rockburst of underground opening triggered by dynamic disturbance," *Tunnelling and Underground Space Technology*, vol. 25, no. 5, pp. 587–599, 2010.

[38] C. Zhang, Z. Ren, D. Hao, and T. Zhang, "Numerical simulation of particle size influence on the breakage mechanism of broken coal," *Arabian Journal for Science and Engineering*, vol. 45, no. 11, pp. 9171–9185, 2020.

[39] C. Zhang, J. Liu, Y. Zhao, P. Han, and L. Zhang, "Numerical simulation of broken coal strength influence on compaction characteristics in goaf," *Natural Resources Research*, vol. 29, pp. 2495–2511, 2020.

[40] X. Chen, Z. Liao, and X. Peng, "Deformability characteristics of jointed rock masses under uniaxial compression," *International Journal of Mining Science and Technology*, vol. 22, no. 2, pp. 213–221, 2012.

[41] B.-R. Chen, X.-T. Feng, Q.-P. Li, R.-Z. Luo, and S. Li, "Rock burst intensity classification based on the radiated energy with damage intensity at Jinping II hydropower station, China," *Rock Mechanics and Rock Engineering*, vol. 48, no. 1, pp. 289–303, 2015.

[42] Y. Liu, F. Dai, T. Zhao, and N.-W. Xu, "Numerical investigation of the dynamic properties of intermittent jointed rock models subjected to cyclic uniaxial compression," *Rock Mechanics and Rock Engineering*, vol. 50, no. 1, pp. 89–112, 2017.

[43] K.-H. Park and Y.-J. Kim, "Analytical solution for a circular opening in an elastic-brittle-plastic rock," *International Journal of Rock Mechanics and Mining Sciences*, vol. 43, no. 4, pp. 616–622, 2006.

[44] M. R. Zareifard and A. Fahimifar, "Analytical solutions for the stresses and deformations of deep tunnels in an elastic-brittle-plastic rock mass considering the damaged zone," *Tunnelling and Underground Space Technology*, vol. 58, pp. 186–196, 2016.

[45] C. Zhang, X. Xu, X. Wang, and Q. Zhao, "Elastic-brittle-plastic mechanical model for rock with confining pressure," *Journal of Mining & Safety Engineering*, vol. 32, no. 1, pp. 132–137, 2015.

[46] C. Zhang, F. Tahmasebinia, I. Canbulat, O. Vardar, and S. Saydam, "Analytical determination of energy release in a coal mass," *Energies*, vol. 11, no. 2, p. 285, 2018.

[47] D. M. Ivars, M. E. Pierce, C. Darcel et al., "The synthetic rock mass approach for jointed rock mass modelling," *International Journal of Rock Mechanics and Mining Sciences*, vol. 48, no. 2, pp. 219–244, 2011.

[48] D. Huang, J. Wang, and S. Liu, "A comprehensive study on the smooth joint model in DEM simulation of jointed rock masses," *Granular Matter*, vol. 17, no. 6, pp. 775–791, 2015.